

# Sds22 and Repo-Man stabilize chromosome segregation by counteracting Aurora B on anaphase kinetochores

Claudia Wurzenberger,<sup>1</sup> Michael Held,<sup>1</sup> Michael A. Lampson,<sup>2</sup> Ina Poser,<sup>3</sup> Anthony A. Hyman,<sup>3</sup> and Daniel W. Gerlich<sup>1</sup>

<sup>1</sup>Institute of Biochemistry, Swiss Federal Institute of Technology Zurich, CH-8093 Zurich, Switzerland

<sup>2</sup>Department of Biology, University of Pennsylvania, Philadelphia, PA 19104

<sup>3</sup>Max Planck Institute for Molecular Cell Biology and Genetics, D-01307 Dresden, Germany

**D**uring mitotic spindle assembly, Aurora B kinase is part of an error correction mechanism that detaches microtubules from kinetochores that are under low mechanical tension. During anaphase, however, kinetochore–microtubule attachments must be maintained despite a drop of tension after removal of sister chromatid cohesion. Consistent with this requirement, Aurora B relocates away from chromosomes to the central spindle at the metaphase–anaphase transition. By ribonucleic acid interference screening using a phosphorylation

biosensor, we identified two PP1-targeting subunits, Sds22 and Repo-Man, which counteracted Aurora B–dependent phosphorylation of the outer kinetochore component Dsn1 during anaphase. Sds22 or Repo-Man depletion induced transient pauses during poleward chromosome movement and a high incidence of chromosome missegregation. Thus, our study identifies PP1-targeting subunits that regulate the microtubule–kinetochore interface during anaphase for faithful chromosome segregation.

## Introduction

Aurora B is the catalytic subunit of the chromosomal passenger complex, which regulates mitotic spindle assembly and cytokinesis (Ruchaud et al., 2007). During mitotic spindle assembly, centromere-localized Aurora B destabilizes kinetochore–microtubule interactions that are under low mechanical tension (Tanaka et al., 2002; Hauf et al., 2003; Lampson et al., 2004; Lampson and Cheeseman, 2011) by phosphorylating several components of the outer kinetochore, including NDC80/HEC1, KNL-1, and Dsn1 (Welburn et al., 2010; DeLuca et al., 2011). The Aurora B–mediated error correction is important for bipolar attachment of all chromosomes, which satisfies the spindle assembly checkpoint to initiate anaphase (Musacchio and Salmon, 2007).

Loss of sister chromatid cohesion at anaphase onset reduces the mechanical tension on kinetochores, yet, kinetochores need to remain attached to microtubules until complete segregation. Removal of Aurora B from centromeres at anaphase onset, regulated by a drop in Cdk1 activity (Pereira and Schiebel, 2003; Gruneberg et al., 2004; Hümmel and Mayer, 2009; Oliveira et al.,

2010), the p97 system (Ramadan et al., 2007), and the E3 ubiquitin ligase Cul3 (Sumara et al., 2007), may explain why anaphase kinetochores are not sensed and detached despite low tension. Supporting this idea, elevated Aurora B levels on anaphase chromosomes lead to untimely spindle checkpoint reengagement (Mirchenko and Uhlmann, 2010; Vázquez-Novelle and Petronczki, 2010), and premature removal of cohesin from metaphase chromosomes in *Drosophila melanogaster* embryos results in irregular chromosome segregation (Oliveira et al., 2010). This suggests that Aurora B removal from anaphase chromosomes is necessary for unperturbed segregation. However, Aurora B may still reach distant targets on anaphase chromatin through a spatial gradient of activity emerging from the central spindle (Fuller et al., 2008).

The regulation of anaphase kinetochores likely involves yet unknown phosphatases. PP1 phosphatase counteracts Aurora B on chromosome arms (Murnion et al., 2001; Sugiyama et al., 2002; Wang et al., 2008), and PP1 also targets to kinetochores

Correspondence to Daniel W. Gerlich: [daniel.gerlich@imba.oeaw.ac.at](mailto:daniel.gerlich@imba.oeaw.ac.at)

D.W. Gerlich's present address is Institute of Molecular Biotechnology of the Austrian Academy of Sciences, 1030 Vienna, Austria.

Abbreviations used in this paper: BAC, bacterial artificial chromosome; FRET, fluorescence resonance energy transfer.

© 2012 Wurzenberger et al. This article is distributed under the terms of an Attribution–Noncommercial–Share Alike–No Mirror Sites license for the first six months after the publication date (see <http://www.rupress.org/terms>). After six months it is available under a Creative Commons License (Attribution–Noncommercial–Share Alike 3.0 Unported license, as described at <http://creativecommons.org/licenses/by-nc-sa/3.0/>).

Supplemental Material can be found at:  
<http://jcb.rupress.org/content/suppl/2012/07/12/jcb.201112112.DC1.html>  
 Original image data can be found at:  
<http://jcb-dataviewer.rupress.org/jcb/browse/5523>

by binding to CENP-E (Kim et al., 2010), KNL-1 (Liu et al., 2010), and Sds22 (Posch et al., 2010). During spindle assembly, PP1 stabilizes microtubule binding at kinetochores in mammalian tissue culture cells (Liu et al., 2010; Posch et al., 2010), as does the budding yeast homolog Glc-7 on reconstituted kinetochores (Sassoon et al., 1999). During anaphase, the regulatory subunit Repo-Man recruits PP1 $\gamma$  to chromatin (Trinkle-Mulcahy et al., 2006), which reverts Haspin- and Aurora B-dependent phosphorylations on histone 3 (Qian et al., 2011; Vagnarelli et al., 2011). Whether these or any other phosphatases regulate the kinetochore-microtubule interface during anaphase is not known. Here, we identify and characterize two PP1-targeting subunits, Repo-Man and Sds22, which regulate the kinetochore-microtubule interface during anaphase to ensure faithful chromosome segregation.

## Results and discussion

To screen for phosphatases counteracting Aurora B during anaphase, we used a fluorescence resonance energy transfer (FRET) biosensor for Aurora B substrate phosphorylation (Fuller et al., 2008). A conformational change in the biosensor upon Aurora B phosphorylation reduces FRET between a CFP for energy transfer (CyPet) donor and a YFP for energy transfer (YPet) acceptor (Fuller et al., 2008). To quantify phosphorylation levels of the biosensor at specific stages of mitosis, we recorded YPet and CyPet emission images of unsynchronized live HeLa Kyoto cells stably expressing a chromatin-targeted version of the biosensor (Fuller et al., 2008) and classified mitotic stages based on chromatin morphology using in-house-developed, supervised machine-learning methods (CellCognition; Fig. 1, A and B; Held et al., 2010). The fully automated assay was validated by RNAi depletion of Aurora B (Fig. S1, A and B), which efficiently inhibited biosensor phosphorylation in mitotic cells (Fig. 1, C–E).

Three different siRNA oligonucleotides targeting each of a genome-wide set of 225 annotated human phosphatases, including catalytic, regulatory, and scaffold subunits (Schmitz et al., 2010), were transfected individually into the reporter cells. Candidate hits that caused biosensor hyperphosphorylation in late anaphase cells 42 h after transfection were ranked based on mean z scores calculated per target gene from all respective siRNA oligonucleotides and two experimental replicates (Fig. 1 F and Table S1). The five top-scoring target genes encode Repo-Man (also termed CDCA2), Sds22 (also termed PPP1R7), PPP2CA, PPP2R1A, and PPP2R2A (also termed B55 $\alpha$ ).

Repo-Man is a PP1-targeting subunit, which had previously been shown to counteract Aurora B on anaphase chromatin (Trinkle-Mulcahy et al., 2006; Qian et al., 2011; Vagnarelli et al., 2011). Sds22 had previously been shown to target PP1 to kinetochores during preanaphase stages to regulate Aurora B (Posch et al., 2010). Three other PP1-targeting subunits, PPP1R3C, PPP1R12A (also termed MYPT1), and PPP1R2 (also termed inhibitor 2), also scored relatively high in the RNAi screen (Table S1), yet, they were not further analyzed in this study. PPP2CA, PPP2R1A, and PPP2R2A form a heterotrimeric PP2A complex that reverts Cdk1 substrate phosphorylations during mitotic exit (Mochida et al., 2009; Schmitz et al., 2010). Several siRNAs caused decreased biosensor

phosphorylation (Fig. 1 F and Table S1), yet, they were not further considered in our study, which aims at the identification of phosphatases counteracting Aurora B.

To validate the phenotypes of the top-ranking candidate hits, we first measured siRNA target protein levels (Fig. S1). Three different siRNAs depleted Repo-Man to 7–13% (Fig. S1, C and D), whereas Sds22 was only reduced to ~50% by three different siRNAs (Fig. S1, E and F). Confocal time-lapse imaging showed that depletion of Repo-Man or Sds22 by any of the different siRNA oligonucleotides delayed dephosphorylation of the biosensor ( $n \geq 12$  cells; Fig. 2 [A–C] and Videos 1–3). Low variability between individual cells (Fig. S2, A and B) suggests that residual protein levels (Fig. S1) are distributed relatively homogeneously within the cell population. Codepletion of Sds22 and Repo-Man further delayed dephosphorylation of the biosensor (Fig. 2 E).

RNAi depletion of PP1 catalytic subunits PP1 $\alpha$  or PP1 $\gamma$  (Fig. S1, G–L) also caused delayed biosensor dephosphorylation ( $n \geq 7$  cells; Fig. S2 C), consistent with the proposed function of Repo-Man and Sds22 as PP1-targeting subunits (Ohkura and Yanagida, 1991; Stone et al., 1993; MacKelvie et al., 1995; Renouf et al., 1995; Dinischiotu et al., 1997; Trinkle-Mulcahy et al., 2006). Even though depletion of PP1 $\beta$  alone had little effect, its codepletion with the two other PP1 catalytic subunits (Fig. S1, G–L) further increased the delay in biosensor dephosphorylation (Fig. S2 C), suggesting functional redundancy between PP1 catalytic subunits that may conceal strong phenotypes after individual subunit depletion. In conclusion, PP1 and its targeting subunits Repo-Man and Sds22 contribute to timely Aurora B substrate dephosphorylation on anaphase chromatin.

Confocal time-lapse imaging of cells in which the PP2A catalytic (PPP2CA), scaffold (PPP2R1A), or regulatory (PPP2R2A/B55 $\alpha$ ) subunits were depleted individually or altogether (Fig. S1, M–R), however, could not confirm their requirement for timely Aurora B biosensor dephosphorylation ( $n \geq 18$  cells; Fig. S2 D). We suspect that the false-positive scoring in our primary screen may have been caused by misclassification of mitotic stages owing to perturbed chromatin morphology (Schmitz et al., 2010). Because all of the other PP2A regulatory subunits scored within the SD of the screening dataset, we conclude that PP2A is not rate limiting for Aurora B substrate dephosphorylation on anaphase chromatin at the protein depletion levels achieved in our RNAi experiments.

The delayed biosensor dephosphorylation in Sds22 or Repo-Man RNAi cells may be caused by incomplete Aurora B removal from chromatin or by inefficient dephosphorylation of its substrates. Confocal imaging of HeLa cells stably expressing Aurora B–EGFP from its endogenous promoter (Poser et al., 2008) showed that neither Repo-Man nor Sds22 RNAi affected Aurora B localization, in contrast to an Mklp2 RNAi-positive control (Fig. 3, A and B; Gruneberg et al., 2004; Hümmel and Mayer, 2009). Immunofluorescence staining by phosphospecific antibodies against the autophosphorylation site Thr232 on Aurora B (an essential activation site; Yasui et al., 2004; Sessa et al., 2005; Ruchaud et al., 2007) and INCENP phosphorylated on Ser893/Ser894 (Aurora B-dependent phosphorylation sites essential for full Aurora B activation; Bishop and Schumacher,

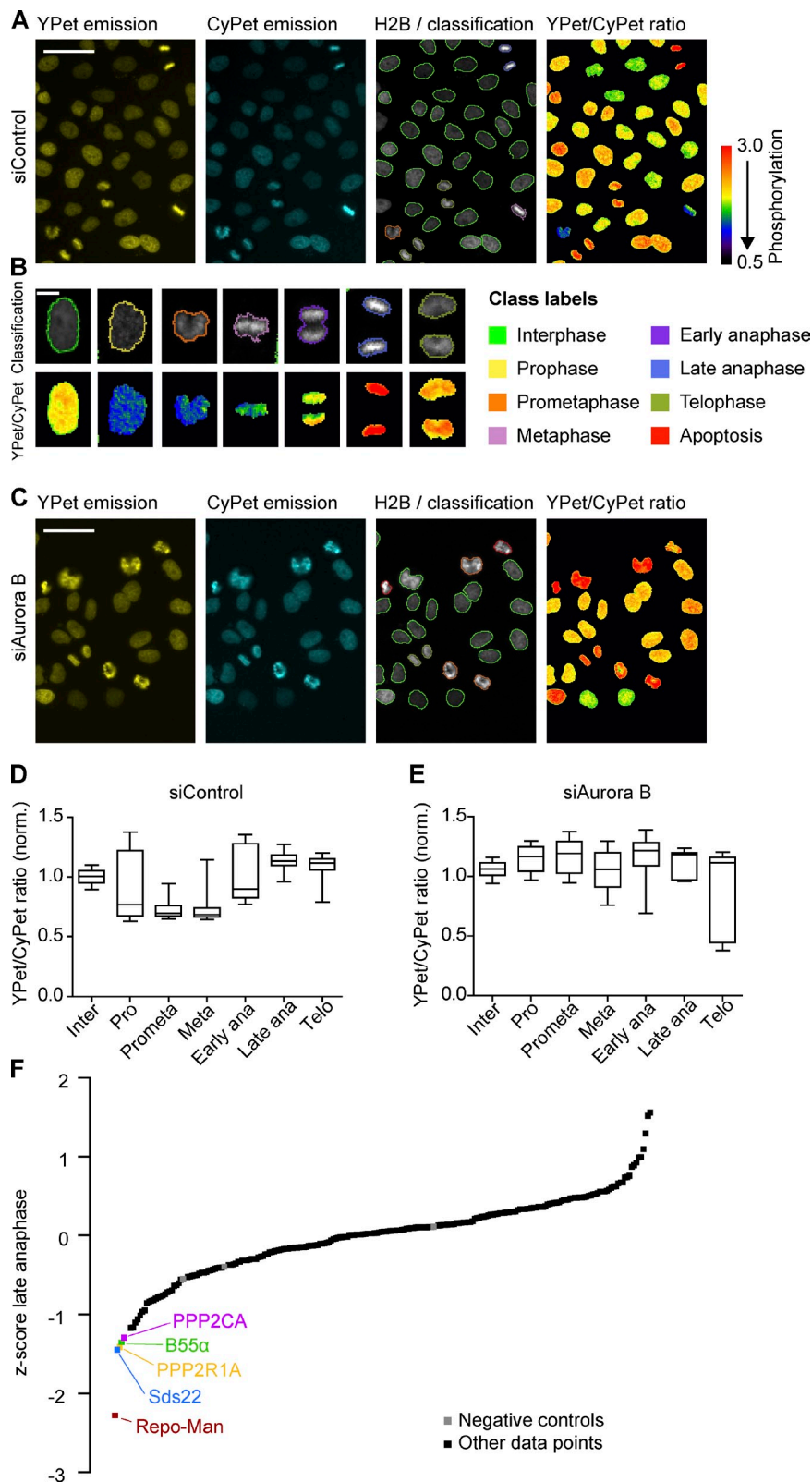


**Figure 1. FRET biosensor-based RNAi screen for Aurora B-counteracting phosphatases.** (A) Live-cell assay for Aurora B phosphorylation. Live HeLa Kyoto cells stably expressing a histone 2B (H2B)-targeted Aurora B FRET biosensor (Fuller et al., 2008) were excited with 426–440-nm light. Pseudocolored YPet/CyPet emission ratios indicate phosphorylation of the biosensor (low ratios indicate high phosphorylation). Mitotic stages were classified by supervised machine learning (Held et al., 2010), as indicated by colored contours. Nontargeting control siRNA (siControl) was transfected 42 h before imaging. Bar, 50  $\mu$ m. (B) Enlarged images of mitotic cells. Bar, 10  $\mu$ m. (C) Cells imaged, as in A, 42 h after transfection of Aurora B-targeting siRNA (siAurora B). Bar, 50  $\mu$ m. (D and E) Statistical analysis of Aurora B biosensor phosphorylation. YPet/CyPet emission ratios were calculated for individual cells, and all measurements were then normalized (norm.) to the median of interphase control cells. Median (line), quartiles (boxes), and 10–90% data range (error bars) indicate YPet/CyPet ratios at different mitotic stages. (D) Biosensor phosphorylation of control cells transfected with nontargeting siRNA. (E) Aurora B RNAi cells. (F) Screen of an siRNA library targeting a genome-wide set of human phosphatases. FRET biosensor phosphorylation in late anaphase cells was assayed as in A–E. Data points represent mean z scores of YPet/CyPet emission ratios in late anaphase for three different siRNAs targeting per gene and two independent experimental replicates. Low z scores indicate hyperphosphorylation of the FRET biosensor.

2002; Honda et al., 2003; Sessa et al., 2005; Salimian et al., 2011) showed that Sds22 or Repo-Man RNAi did not affect the levels of active Aurora B on anaphase chromosomes (Figs. 3 [C–E] and S2 [E–G]). Thus, Repo-Man and Sds22 contribute to anaphase dephosphorylation of chromosomal Aurora B sites independent of Aurora B translocation or inactivation.

Elevated Aurora B levels on anaphase chromatin in Mklp2 RNAi cells correlated with delayed dephosphorylation of the chromatin-targeted biosensor (Fig. 2 D). The delay was further increased by codepleting Sds22 or Repo-Man (Fig. 2 E), yet, biosensor dephosphorylation reached similar levels as in control cells  $\sim$ 15 min after anaphase onset, despite the persistence

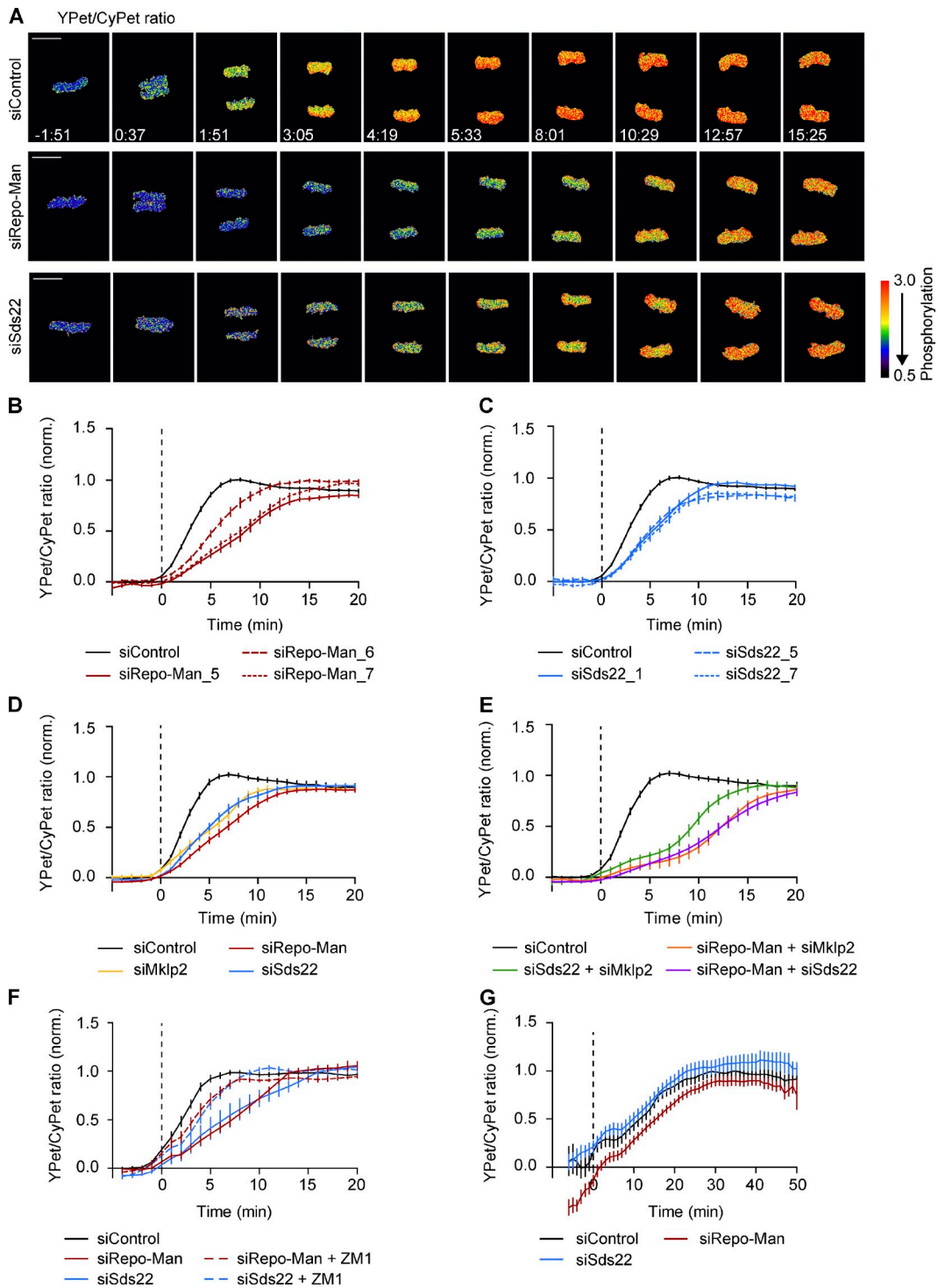


**Figure 2. Repo-Man and Sds22 are required for timely dephosphorylation of the chromatin-targeted FRET biosensor.** (A) Confocal time-lapse images of HeLa Kyoto cells expressing the H2B-targeted Aurora B FRET biosensor, 42 h after transfection of a nontargeting control siRNA (siControl), or siRNAs targeting Repo-Man or Sds22. YPet/CyPet emission ratios are displayed in pseudocolor. Time is shown in min/s. Bars, 10  $\mu$ m. (B–F) Quantification of YPet/CyPet emission ratios from cells, as shown in A, normalized (norm.) to mean YPet/CyPet ratios of control RNAi cells in metaphase. Curves and bars display mean  $\pm$  SEM. Videos were aligned to the onset of chromosome segregation ( $t = 0$  min; dashed lines). (B and C) Phosphorylation of the chromatin-targeted biosensor after transfection of different siRNAs targeting Repo-Man or Sds22.  $n \geq 12$  cells. (D and E) Phosphorylation of the chromatin-targeted biosensor after transfection of siRNAs targeting Mklp2, Repo-Man, or Sds22.  $n \geq 10$  cells. (F) Phosphorylation of the chromatin-targeted biosensor after transfection of siRNAs targeting Repo-Man or Sds22. ZM1 was added to a final concentration of 2  $\mu$ M immediately after the onset of chromosome segregation.  $n \geq 14$  cells. (G) Phosphorylation kinetics of a cytoplasmic Aurora B biosensor [Fuller et al., 2008]. Normalized YPet/CyPet emission ratios of live HeLa cells stably coexpressing the cytoplasmic biosensor and H2B-mCherry. Mean  $\pm$  SEM.  $n \geq 18$  cells.  $t = 0$  min at chromosome segregation onset (dashed line).

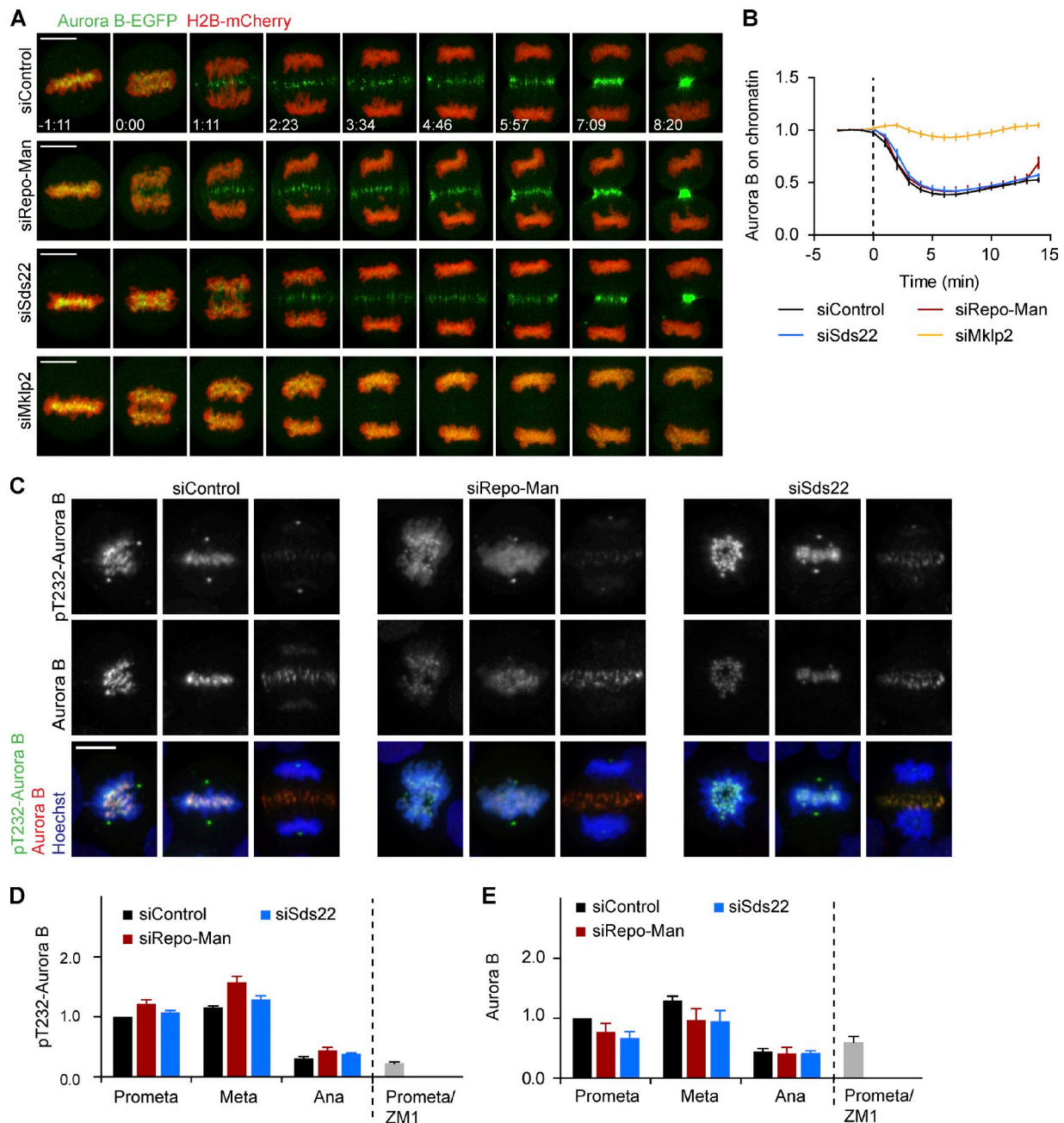


**Figure 3. Repo-Man and Sds22 function downstream of Aurora B.** (A) Confocal time-lapse imaging of HeLa Kyoto cells stably expressing Aurora B-EGFP and H2B-mCherry. Time is shown in min/s.  $t = 0$  min at chromosome segregation onset. Bars, 10  $\mu$ m. (B) Quantification of Aurora B-EGFP levels on chromatin by ratios of mean Aurora B-EGFP fluorescence divided by mean H2B-mCherry fluorescence.  $t = 0$  min at the onset of chromosome segregation (dashed line). Fluorescence ratios of individual cells were normalized to metaphase values.  $n \geq 18$  cells. (C) Immunofluorescence staining with antibodies against Aurora B and Aurora B phosphorylated at Thr232 (pT232). DNA was stained with Hoechst 33342. Representative example images of prometaphase, metaphase, and anaphase cells 42 h after transfection with control, Repo-Man, or Sds22 RNAi are shown. Bar, 10  $\mu$ m. (D and E) Quantification of Thr232-phosphorylated Aurora B (D) or total Aurora B (E) on chromatin in immunofluorescence images, as shown in C. Fluorescence intensities were normalized to control siRNA-transfected prometaphase cells. The dashed lines separate measurements of phospho-Aurora B levels on chromatin in the different siRNA conditions (left) from ZM1 treatment (inhibitor of Aurora B kinase, used as a positive control). Mean  $\pm$  SEM.  $n = 7$  (D) or 4 (E) independent experiments ( $>120$  [D] or  $>70$  [E] cells per experimental condition).

of high levels of Aurora B on chromatin at these late time points (compare Fig. 3 [A and B] with Fig. 2 E). The phosphatase activity that eventually dephosphorylates the biosensor in this experiment may emerge from residual amounts of the respective RNAi target proteins, from functional redundancy between Sds22 and Repo-Man, or from unknown other phosphatases.

Sds22 and Repo-Man may dephosphorylate chromosomal Aurora B substrates that had been phosphorylated before re-location of the kinase to the central spindle or counteract a sustained Aurora B activity emerging from the central spindle via a long-range spatial gradient (Fuller et al., 2008) or from residual Aurora B on anaphase chromatin. Aurora B inhibition by

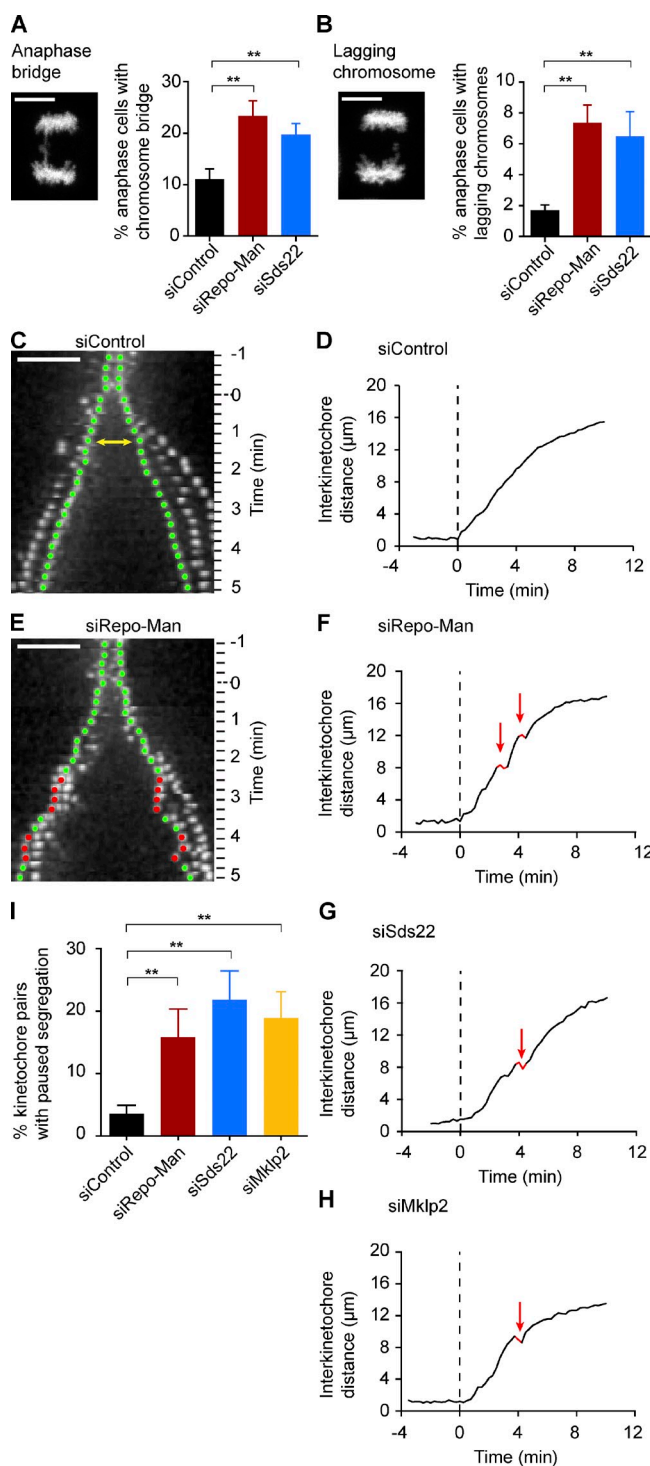


**Figure 4. Repo-Man and Sds22 stabilize anaphase chromosome segregation.** (A and B) Depletion of Repo-Man or Sds22 increases the incidence of anaphase bridges (A) and lagging chromosomes (B). Segregation defects were detected in confocal videos of live HeLa Kyoto cells stably expressing H2B-mCherry ( $n > 500$  cells; seven independent experiments; \*\*,  $P < 0.001$ , using a two-sided binomial test). Bars, 10  $\mu\text{m}$ . (C–I) 3D tracking of kinetochores in HeLa cells stably expressing EGFP-CENP-A (Jaqaman et al., 2010) reveals pauses in poleward segregation. (C and E) Kymographs of sister kinetochore pairs (yellow arrow highlights interkinetochore distance). Tracked sister kinetochores are highlighted by colored circles; green represents linear segregation, and red represents paused segregation (net movement of  $< 0.1 \mu\text{m}$  in three subsequent frames).  $t = 0$  min at chromosome segregation onset (dashed lines). Bars, 5  $\mu\text{m}$ . (D, F, G, and H) 3D interkinetochore distances of sister kinetochore pairs from metaphase

ZM1 (Girdler et al., 2006) briefly after anaphase onset significantly accelerated biosensor dephosphorylation in Repo-Man and Sds22 RNAi cells (Fig. 2 F), indicating that Aurora B continues to regulate substrate phosphorylation on chromosomes after anaphase onset. This could be either by direct substrate phosphorylation on chromosomes or indirectly by regulating counteracting phosphatases.

Sds22 or Repo-Man RNAi had minor effects on dephosphorylation of a cytoplasmic Aurora B phosphorylation FRET biosensor (Fig. 2 G; Fuller et al., 2008). This suggests that Sds22 and Repo-Man act locally on chromosomes, which is in accordance with their reported localization to kinetochores and chromatin, respectively (Trinkle-Mulcahy et al., 2006; Posch et al., 2010).

To investigate the relevance of timely Aurora B substrate dephosphorylation, we recorded 3D confocal live-cell videos from HeLa cells stably expressing H2B-mCherry. Repo-Man or Sds22 depletion significantly increased the frequency of anaphase bridges and lagging chromosomes ( $n > 500$  cells in seven independent experiments;  $P < 0.001$ , using a two-sided binomial test; Fig. 4, A and B). To test for on-target specificity of the phenotype, we transfected siRNAs specific for human Repo-Man or Sds22 in HeLa cell lines stably expressing the respective siRNA-resistant, EGFP-tagged mouse counterparts (Fig. S3, A–D). Depletion of endogenous human Repo-Man or Sds22 in the cell lines expressing the corresponding mouse genes did not significantly increase the frequency of chromosome missegregation (Fig. S3, E and F). Thus, chromosome missegregation results from on-target depletion of Repo-Man or Sds22.

Chromosome missegregation may result from defects before anaphase onset, like chromosome misattachment during early mitosis or cytokinesis failure in preceding cell divisions. The fraction of binucleated cells was not increased in cells depleted of Sds22 or Repo-Man ( $3.1 \pm 0.5\%$  in control RNAi cells,  $2.8 \pm 0.7\%$  in Repo-Man RNAi cells, and  $3.1 \pm 0.3\%$  in Sds22 RNAi cells;  $n > 1,900$  cells per condition), indicating effective cytokinesis. We detected a small increase in chromosome misalignment in cells depleted of Sds22 ( $5.4 \pm 1.8\%$  compared with  $4.5 \pm 0.7\%$  in control RNAi or  $4.2 \pm 1.0\%$  in Repo-Man RNAi cells;  $n > 400$  cells), yet, this fraction is much smaller than the fraction of cells with anaphase segregation errors (Fig. 4, A and B).

To gain more insight into the chromosome missegregation phenotype, we tracked kinetochores in 3D videos of live HeLa cells stably expressing EGFP-CENP-A (Jaqaman et al., 2010). By measuring sister kinetochore distances, we determined segregation dynamics independent of spindle rotation and translation (Fig. 4, C and D). Repo-Man or Sds22 depletion had only a weak effect on the overall mean segregation speed (Fig. S3 G).

until full segregation. Paused segregation (net movement of  $< 100$  nm in three subsequent frames) is highlighted in red.  $t = 0$  min at chromosome segregation onset (dashed lines). (I) Incidence of sister kinetochore pairs per cell with paused segregation after initially normal segregation during poleward movement 0–5 min after anaphase onset.  $n \geq 9$  cells (10 kinetochore pairs per cell) per condition. Mean  $\pm$  SEM. \*\*,  $P < 0.001$ , using a two-sided binomial test.

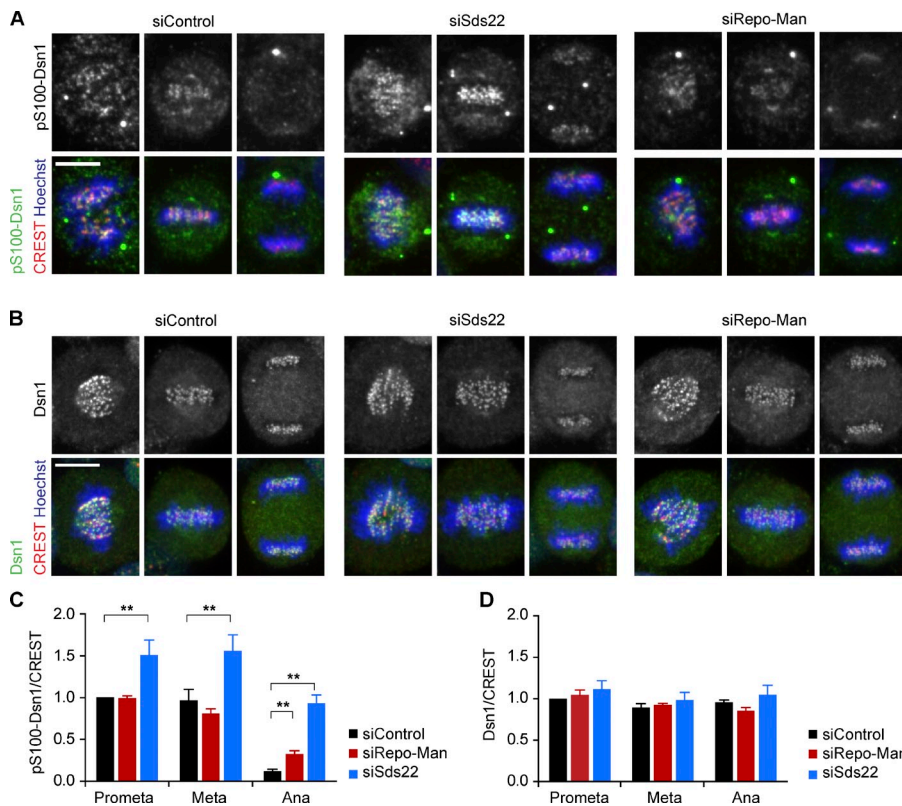


**Figure 5. Repo-Man and Sds22 are required for timely dephosphorylation of the microtubule attachment factor Dsn1.** (A and B) Immunofluorescence staining with an antibody against Dsn1 phosphorylated at Ser100 (pS100; Welburn et al., 2010; A) or total Dsn1 (Kline et al., 2006; B). Representative example images of cells costained for pSer100 Dsn1 (A) or Dsn1 (B), kinetochores (CREST), and DNA (Hoechst 33342). Bars, 10  $\mu$ m. (C and D) Quantification of phosphorylated Dsn1 or total Dsn1 on kinetochores. pSer100 Dsn1/CREST or Dsn1/CREST fluorescence intensity ratios were normalized to control siRNA-transfected prometaphase cells. Mean  $\pm$  SEM.  $n = 3$  experiments (>30 cells per experimental condition; 16 kinetochores per cell). \*\*,  $P < 0.001$ , using a two-tailed Student's  $t$  test.

However, a large fraction of individual kinetochores temporarily paused segregation or even transiently moved backward in cells depleted of Sds22 or Repo-Man (Fig. 4, C–I). The segregation pauses occurred at variable timing after anaphase onset, did not correlate with increased spindle rotation (Fig. S3, H–K), and were not simultaneously observed on adjacent chromosomes, indicating that irregular segregation results from a defect at individual chromosomes rather than an overall perturbation of the spindle.

To investigate whether the observed segregation defects may be a consequence of misregulated Aurora B substrate phosphorylation, we maintained high levels of Aurora B on anaphase chromatin using Mklp2 RNAi (Figs. 2 D and 3 [A and B]; Gruneberg et al., 2004; Hümmel and Mayer, 2009). Indeed, Mklp2 RNAi also induced transient pauses in poleward segregation (Figs. 4 [H and I] and S3 K), consistent with a requirement for timely Aurora B substrate dephosphorylation for steady chromosome segregation.

Pauses in chromosome segregation may be caused by defective chromosome structure, incomplete resolution of sister chromatid arms, or by destabilized kinetochore–microtubule interactions. In metaphase, the kinetochore–microtubule affinity is regulated by differential phosphorylation of Aurora B sites on outer kinetochore components (Welburn et al., 2010; DeLuca et al., 2011). Ser100-phosphorylated Dsn1 (Welburn et al., 2010) was indeed elevated on anaphase kinetochores of Repo-Man or Sds22 RNAi cells (Fig. 5, A and C), whereas total Dsn1 levels were unaffected (Fig. 5, B and D).

Misregulated phosphorylation of the kinetochore–microtubule interface may explain the segregation defects observed in Repo-Man and Sds22 RNAi cells. However, other

defects like incompletely resolved sister chromatids may also contribute to chromosome segregation pauses. A previous study reported decreased phosphorylation levels of several Aurora B substrates in Sds22-depleted metaphase cells (Posch et al., 2010). In contrast, Dsn1 Ser100 phosphorylation was significantly elevated during prometaphase and metaphase in Sds22 RNAi cells (Fig. 5 C). Even though the mechanism underlying differential regulation of Aurora B substrates by Sds22 is unclear, we also observed that depletion of Sds22, but not of Repo-Man, delayed progression from mitotic entry until anaphase, as previously reported (Fig. S3 L; Posch et al., 2010).

Our data indicate that the PP1-targeting subunits Repo-Man and Sds22 contribute to faithful chromosome segregation. Repo-Man and Sds22 counteract a sustained activity of Aurora B on anaphase chromatin and on kinetochores after translocation of the chromosomal passenger complex to the central spindle. Thus, a balance between opposing kinase and phosphatase activities shapes the spatial gradient of Aurora B–dependent phosphorylation on anaphase chromatin (Fuller et al., 2008). This is in agreement with previous studies reporting that PP1 counteracts Aurora B in vitro and during chromosome alignment (Murnion et al., 2001; Sugiyama et al., 2002; Wang et al., 2008; Kim et al., 2010; Liu et al., 2010; Posch et al., 2010).

Our high-resolution tracking of segregating chromosomes shows that oscillatory chromosome dynamics observed in metaphase (Jaqaman et al., 2010) switch to a steady linear movement during anaphase. Therefore, the drop in mechanical tension at anaphase onset does not destabilize microtubule attachments in cells, as observed with in vitro reconstituted kinetochores (Akiyoshi et al., 2010). Transient segregation pauses in Repo-Man and Sds22 RNAi cells could arise from defects in microtubule

flux or depolymerization (Civelekoglu-Scholey and Scholey, 2010; Walczak et al., 2010). A perturbed chromosome architecture, as reported for Repo-Man-deficient cells (Vagnarelli et al., 2006), could further contribute to segregation errors.

Chromosome missegregation leads to aneuploidy, a potentially carcinogenic state (Ganem et al., 2007). Previous studies on the mechanisms ensuring faithful chromosome segregation mainly focused on the spindle checkpoint and error correction machinery (Musacchio and Salmon, 2007; Lampson and Cheeseman, 2011). Less well characterized but equally important for faithful chromosome segregation is an unperturbed anaphase. Our study provides new insight into the regulation of anaphase chromosome segregation and reveals the diversity of phosphatases coordinating the different events of mitotic exit.

## Materials and methods

### Cell lines and plasmids

The HeLa Kyoto cell line was obtained from S. Narumiya (Kyoto University, Kyoto, Japan) and cultured in DME (Gibco) supplemented with 10% (vol/vol) FBS (PAA Laboratories) and 1% (vol/vol) penicillin-streptomycin (Invitrogen). Monoclonal reporter cell lines were generated as previously described (Schmitz and Gerlich, 2009). All reporter cell lines used in this study showed similar proliferation rates as HeLa Kyoto wild-type cells.

The chromatin-targeted FRET biosensor (Fuller et al., 2008) was N-terminally fused to full-length core histone 2B (H2B) and was subcloned into the pRESpuo2 vector (Takara Bio Inc.). The cytoplasmic FRET biosensor was generated by removing the N-terminal H2B sequence.

Other monoclonal cell lines used in this study stably expressed full-length H2B C-terminally fused to mCherry (H2B-mCherry; Steigemann et al., 2009), full-length CENP-A N-terminally fused to EGFP (EGFP-CENP-A; obtained by P. Meraldi, Swiss Federal Institute of Technology Zurich, Zurich, Switzerland; Jaqaman et al., 2010), or coexpressed H2B-mCherry and importin- $\beta$ -binding domain of importin- $\alpha$  (IBB) C-terminally fused to EGFP (IBB-EGFP; Schmitz et al., 2010).

Murine bacterial artificial chromosomes (BACs; RP23-41716 [AURKB], RP23-316017 [Sds22/PPP1R7], and RP24-290N12 Repo-Man/CDCA2) harboring the genes of interest were obtained from the BACPAC Resources Center. Mouse Sds22 protein has 94% amino acid sequence identity with the human homolog, and mouse Repo-Man protein has 53% amino acid sequence identity with the human homolog. The N-terminal NFLAP (EGFP-Neo) or LAP (EGFP-IRES-Neo) cassette was PCR amplified using primers that carry 50 nucleotides of homology to the N terminus (Repo-Man) or C terminus (Aurora B and Sds22) of the target genes. Recombineering and stable transfection of the modified BAC was performed as previously described (Poser et al., 2008). In brief, both a plasmid carrying two recombinases and the purified tagging cassette were introduced into the *Escherichia coli* strain containing the BAC vector using electroporation. Precise incorporation of the tagging cassette was confirmed by PCR and sequencing. GFP-tagged BACs were isolated from bacteria and transfected into HeLa Kyoto cells using Effectene (QIAGEN). Pools of HeLa cells stably expressing the GFP-tagged transgenes were selected by cultivation in selection media containing 400  $\mu$ g/ml geneticin (G418; Invitrogen) and were analyzed by Western blot and immunofluorescence using an anti-GFP antibody (Roche) to verify correct protein size and localization of the tagged protein.

The cell pools stably expressing tagged mouse Sds22 or Repo-Man proliferated at normal rate and did not show elevated levels of apoptosis. The incidence of chromosome missegregation was similar to control cells in mouse Sds22-expressing cell pools, yet, it was increased to ~20% in cell pools stably expressing mouse Repo-Man. Cell pools stably expressing BAC transgenes of Aurora B, Sds22, and Repo-Man were cotransfected with H2B-mCherry and selected for monoclonal cell lines stably coexpressing both genes of interest.

### siRNA transfection

The human siRNA phosphatase library was as published in Schmitz et al. (2010). siRNAs targeting PP1 catalytic subunits, Repo-Man, Sds22, and Mklp2 were obtained from QIAGEN and are listed in Table 1. The nontargeting control siRNA used was AllStars (QIAGEN). siRNA duplexes were

transfected ~42 h before analysis in 96-well plastic-bottom plates ( $\mu$ clear; Greiner Bio-One Ltd.), chambered coverslips (LabTek; Thermo Fisher Scientific), or multiwell tissue culture dishes (Thermo Fisher Scientific) by reverse transfection using Oligofectamine (Invitrogen), according to the manufacturer's instructions. Final siRNA concentration was 50 nM.

### Inhibitor treatment

For inhibition of Aurora B in quantitative immunofluorescences, ZM1 was added to a final concentration of 2  $\mu$ M 1 h before fixation. For anaphase-specific inhibition of Aurora B during time-lapse imaging, ZM1 (Tocris Bioscience) was prediluted to 20  $\mu$ M stock solution in prewarmed imaging medium and added directly after chromosome segregation to a final concentration of 2  $\mu$ M.

### Live-cell microscopy

Cells were grown in 96-well plastic-bottom plates ( $\mu$ clear) or chambered coverslips (LabTek). Imaging was performed in DME containing 10% (vol/vol) FBS and 1% (vol/vol) penicillin-streptomycin without phenol red and riboflavin or in Leibovitz's L-15 medium (Gibco) containing 10% (vol/vol) FBS and 1% (vol/vol) penicillin-streptomycin.

Automated imaging for RNAi screening was performed on a screening microscope (ImageXpress Micro; Molecular Devices) equipped with a reflection-based laser autofocus, a CoolSNAP HQ camera (Roper Scientific), and CFP-YFP FRET filters for sensitized emission ratio imaging (excitation filter of 426–440 nm and emission filters of 467–492 nm [CFP] or 529–556 nm [YFP]) using a 10 $\times$  0.5 NA Fluor-S dry objective (Nikon) and controlled by in-house-developed MetaMorph macros (Held et al., 2010). Cells were maintained at 37°C in a humidified atmosphere of 5% CO<sub>2</sub>.

Scanning confocal microscopy was performed on a customized microscope (LSM 510 Axiovert; Carl Zeiss) equipped with piezo focus drive (piezosystem jena GmbH) and custom-designed filters (Chroma Technology Corp.) using a 63 $\times$  1.4 NA oil Plan Apochromat objective or a 40 $\times$  1.3 NA oil differential interference contrast EC Plan Neofluar objective (Carl Zeiss) and controlled by the LSM 510 AIM software. Cells were maintained at 37°C in a humidified atmosphere of 5% CO<sub>2</sub> by an EMBL incubation chamber.

Live-cell imaging of EGFP-CENP-A cells for tracking purposes was performed on a multiplexed system (Olympus IX71 DeltaVision; Applied Precision) equipped with a camera (CoolSNAP HQ2) and temperature incubation, using a 100 $\times$  1.4 NA oil UPlanSApo objective (Olympus) and the softWoRx acquisition software. 20 z sections with a z step of 0.5  $\mu$ m were imaged at a temporal resolution of 15 s. Cells were imaged for a maximum of 5 min before chromosome segregation to reduce phototoxic side effects.

### Immunofluorescence

For immunofluorescence staining, HeLa Kyoto cells were grown in chambered coverslips (LabTek). For staining of Dsn1 and phospho-Ser100 Dsn1, cells were preextracted for 3 min in PEM buffer (100 mM Pipes, pH 6.9, 10 mM EGTA, and 1 mM MgCl<sub>2</sub>) with 0.4% Triton X-100 and then fixed for 10 min in 4% PFA in PEM with 0.2% Triton X-100. For staining of Aurora B, phospho-Thr232 Aurora B, INCENP, and phospho-Ser893/894 INCENP, cells were fixed for 10 min in PTEMF (4% PFA, 0.2% Triton X-100, 20 mM Pipes, pH 6.9, 10 mM EGTA, and 1 mM MgCl<sub>2</sub>). Cells were blocked in 3% BSA in PBS for 1 h. The primary antibodies used were polyclonal rabbit anti-Dsn1 (1:1,000; Kline et al., 2006) and polyclonal rabbit anti-phospho-Ser100 Dsn1 (1:1,000; Welburn et al., 2010; both gifts from I. Cheeseman, Massachusetts Institute of Technology, Cambridge, MA), human CREST antiserum (1:500; Antibodies Inc.), polyclonal rabbit anti-phospho-Thr232 Aurora B (1:1,000; Rockland Immunochemicals), monoclonal mouse anti-Aurora B (1:250; Abcam), polyclonal rabbit anti-phospho-Ser893/894 INCENP (1:1,000; Salimian et al., 2011), and monoclonal mouse anti-INCENP (1:1,000; Active Motif). Secondary antibodies were Alexa Fluor 488, 568, and 594 conjugates from Invitrogen (1:500). DNA was stained with 0.2  $\mu$ g/ml Hoechst 33342 (Sigma-Aldrich). Images were acquired on a spinning-disk microscope (Nipkow; Carl Zeiss) equipped with a motorized piezo stage (MS-2000; Applied Scientific Instrumentation) and two cameras (Evolve 512; Photometrics) using a 63 $\times$  1.2 NA water C Apochromat M27 objective and the AxioVision software (Carl Zeiss). 20 z sections with a z step of 0.3  $\mu$ m were acquired. All quantitative immunofluorescence experiments were performed in at least three independent experiments, each with two coverslips per experimental condition and replicate. The figures displayed in the manuscript show mean  $\pm$  SEM of individual experiments, which generally showed similar effects, thus validating that the reported effects on antigen abundance are caused by the specific experimental perturbation and not a staining variability between different coverslips.

Table 1. siRNA sequences

Targeted gene	siRNA name	siRNA target sequence
Human Repo-Man	Hs_CDCA2_5	5'-AGCAAATACTCCATTGCGTAA-3'
Human Repo-Man	Hs_CDCA2_6	5'-CAGCCCTGCACTGTATCGAAA-3'
Human Repo-Man	Hs_CDCA2_7	5'-ATGGGACTCATCCGAGCTTAA-3'
Human Sds22	Hs_PPP1R7_1	5'-TTCAGATGCCGTGCAATTA-3'
Human Sds22	Hs_PPP1R7_5	5'-CCAGATCAAGAAGATTGAGAA-3'
Human Sds22	Hs_PPP1R7_7	5'-AGAGTTCTGGATGAACGACAA-3'
Human Mklp2	Hs_Kif20a_5	5'-AAGGCCAGGTTCTGCCAAA-3'
Human PP1 $\alpha$	Hs_PPP1CA_9	5'-CCGCAATCCGCCAAAGCCAA-3'
Human PP1 $\beta$	Hs_PPP1CB_3	5'-TAGGAATATGGTCGGGCTGAA-3'
Human PP1 $\gamma$	Hs_PPP1CC_5	5'-CTGGTTATAACAGCAAATGAA-3'
Human PP2A-B55 $\alpha$	Hs_PPP2AR2A_5	5'-CTGCAGATGATTGCGGATTA-3'
Human PP2A-R1A	Hs_PPP2AR1A_7	5'-GACCAGGATGTGGACGTCAA-3'
Human PP2A-CA	Hs_PPP2ACA_5	5'-ATGGAACCTGACGATACTCTA-3'

### Image analysis

Automated image analysis for FRET biosensor-based screening was performed using the in-house-developed CellCognition software (Held et al., 2010). To compensate for inhomogeneous illumination, images were flatfield corrected by background images acquired in empty wells. Nuclei were segmented by adaptive thresholding, and texture and shape features were calculated for each object, as described in Held et al. (2010). Samples for nine user-defined morphology classes (interphase, prophase, prometaphase, metaphase, early anaphase, late anaphase, telophase, binucleate cells, and apoptotic cells) were annotated manually to train a support vector machine classifier. Supervised classification was then applied to high-throughput screening data. Mean fluorescence intensities were measured in the nuclei, and background-subtracted YPet/CyPet emission ratios were normalized to the mean of all interphase cells of one experimental replicate. Z scores of individual siRNA conditions in late anaphase were calculated as the deviation of mean YPet/CyPet ratios of one condition to the overall mean of all data points of one experimental replicate, normalized to the SD of all data points. Z scores for hit ranking were calculated as the mean of the three siRNAs targeting each gene and both experimental replicates. siRNA conditions with  $n < 15$  late anaphase cells were excluded from further analysis.

Automated timing measurements of mitotic progression from nuclear envelope breakdown to chromosome segregation were performed using the CellCognition software, as previously described (Held et al., 2010; Schmitz et al., 2010). Nuclei were tracked over time and classified based on their chromatin morphology by supervised machine learning. Nuclear envelope breakdown was detected by a decrease in the ratio of the mean nuclear versus cytoplasmic IBB-EGFP fluorescence.

Confocal time-lapse videos of the FRET biosensor were analyzed using ImageJ (National Institutes of Health). Regions of interest were determined by thresholding on the YFP channel, and fluorescence intensities were extracted from mean intensity projections. Background-subtracted YPet/CyPet emission ratios were normalized to late metaphase (1–5 min before onset of chromosome segregation) and late anaphase (6–8 min after onset of chromosome segregation) of control RNAi cells and plotted over time aligned on anaphase onset.

Chromosomal localization of Aurora B–EGFP was analyzed similarly in mean projections of confocal z stacks. Nuclear regions were defined by thresholding on the H2B-mCherry channel, and Aurora B–EGFP mean fluorescence on chromatin was normalized to H2B-mCherry mean fluorescence to compensate for chromosome condensation. Relative Aurora B levels were then calculated individually in each cell relative to mean levels in metaphase to compensate for variable expression levels of the two markers in different cells.

Kinetochore tracking in anaphase was performed using Imaris software (Bitplane). 3D kinetochore positions were automatically determined with subpixel resolution using the Spots function of Imaris. Sister kinetochores were then identified and tracked manually from 2 min before anaphase onset until up to 20 min after anaphase onset. 3D interkinetochore distances were calculated and plotted over time. Mean segregation speed was determined by linear regression of the segregation curve from 0 to 4 min after onset of chromosome segregation. Pausing events were defined as a net movement of  $< 0.1 \mu\text{m}$  between three subsequent frames, and the

frequency of sister kinetochores that displayed paused segregation was scored for 10 kinetochore pairs per cell.

Phospho-Thr232 Aurora B, total Aurora B, phospho-Ser893/894 INCENP, and total INCENP levels on chromatin were measured in mean projections of optical z stacks. Regions of interest were defined by thresholding on the Hoechst channel using ImageJ. Fluorescence intensities were background subtracted and normalized to prometaphase control RNAi cells.

Dsn1 and phospho-Ser100 Dsn1 levels were measured in regions of interest of constant size around single kinetochores (16 kinetochores per cell) in mean projections of z stacks using ImageJ. Fluorescence intensities on the Dsn1, phospho-Dsn1, and CREST channel were background subtracted, and Dsn1/CREST or pSer100 Dsn1/CREST ratios were normalized to control RNAi prometaphase cells. Staining by pSer100 Dsn1 revealed prominent cytoplasmic foci in all RNAi conditions, which were not apparent in stainings for total Dsn1 and therefore likely represent an unspecific cross-reaction of the antibody. We did not measure fluorescence close to cytoplasmic foci.

### Quantitative real-time PCR

Cells were transfected with siRNAs in 12-well plates (Thermo Fisher Scientific) 40 h before RNA isolation by phenol-chloroform extraction using TRIZOL (Invitrogen), according to the manufacturer's instructions. cDNA was synthesized by reverse transcription using random hexamer primers (Microsynth) and M-MuLV reverse transcription (Thermo Fisher Scientific). Real-time PCR was performed on a LightCycler 480 (Roche) using the LightCycler 480 SYBR green I Master Mix (Roche). Efficiency of gene amplification was determined by a standard curve, and expression levels were quantified relative to glyceraldehyde 3-phosphate dehydrogenase levels. Primers were designed using Autoprime software. For amplification of human and mouse Repo-Man or Sds22, specificity of primer sequences was validated by sequence alignment using the BLASTN algorithm. All primer pairs are listed in Table 2.

### Western blotting

Cells were transfected with siRNAs in 6-well plates (Thermo Fisher Scientific) and lysed in 1 $\times$  SDS loading buffer 48 h after transfection. Protein samples were separated by SDS-PAGE and transferred to a polyvinylidene fluoride membrane (EMD Millipore) by semidry blotting. The following primary antibodies were used: polyclonal rabbit anti-Sds22 (a gift from J. Swedlow, University of Dundee, Dundee, Scotland, UK; Posch et al., 2010), polyclonal rabbit anti-Repo-Man (Abcam), polyclonal goat anti-PP1 $\alpha$ , polyclonal goat anti-PP1 $\beta$ , and polyclonal goat anti-PP1 $\gamma$  (all from Santa Cruz Biotechnology, Inc.), monoclonal mouse anti-Aurora B (Abcam), polyclonal rabbit anti-PPP2CA (Cell Signaling Technology), polyclonal rabbit anti-PPP2R1A (Cell Signaling Technology), monoclonal mouse anti-PP2A-B55 $\alpha$  (Santa Cruz Biotechnology, Inc.), and monoclonal mouse anti-actin (EMD Millipore). Quantification of protein concentration was performed on the FluorChem system (Alpha Innotec).

### Online supplemental material

Fig. S1 shows validation of target gene depletion. Fig. S2 shows biosensor phosphorylation kinetics for various experimental conditions and immunofluorescence staining for INCENP phosphorylation. Fig. S3 shows on-target validation of siRNAs by phenotype rescue and spindle rotation

Table 2. Primers for quantitative real-time PCR

Amplified gene	Primer name	Primer sequence
Human Repo-Man	Hs_CDCA2_L	5'-AGAGAGCTTACAGGAACACTG-3'
Human Repo-Man	Hs_CDCA2_R	5'-TTCATCTTCTGCTTCTTCTC-3'
Mouse Repo-Man	Mm_CDCA2_L	5'-TTGCTGAGAAGTCACCTG-3'
Mouse Repo-Man	Mm_CDCA2_R	5'-GCCCTCTACACAGTCAGTC-3'
Human Sds22	Hs_PPP1R7_L	5'-AGAGATGCAGAGGATGTTG-3'
Human Sds22	Hs_PPP1R7_R	5'-CAGCTCTCGAAGACTCTGTAG-3'
Mouse Sds22	Mm_PPP1R7_L	5'-CTGACAGAATTGGAGGTTTC-3'
Mouse Sds22	Mm_PPP1R7_R	5'-GTCAATCCCTCAATGTTTC-3'

and mean segregation velocity measurements. Videos 1–3 show dephosphorylation of the chromatin-targeted Aurora B biosensor during mitotic exit in a control RNAi cell, a Repo-Man RNAi cell, and an Sds22 RNAi cell, respectively. Online supplemental material is available at <http://www.jcb.org/cgi/content/full/jcb.201112112/DC1>.

The authors thank I. Cheeseman for critical comments on the manuscript and J.P. Fededa, S. Noser, N. Mchedlishvili, the Swiss Federal Institute of Technology Zurich Light Microscopy Centre, and the Swiss Federal Institute of Technology Zurich RNAi Screening Centre for excellent technical assistance. We thank P. Meraldi for EGFP-CENP-A-expressing cells, J. Swedlow for anti-Sds22 antibody, and I. Cheeseman for anti-phospho-Ser100 Dsn1 and anti-Dsn1 antibody.

Research in the Gerlich laboratory has received funding from the European Community's Seventh Framework Program FP7/2007-2013 under grant agreements no. 241548 (MitoSys) and no. 258068 (Systems Microscopy) and grants no. 31003A\_129895 and no. PDFMP3\_124904 from the Swiss National Science Foundation. C. Wurzenberger is a fellow of the Zurich PhD Program in Molecular Life Sciences and has received funding from a PhD fellowship by the Boehringer Ingelheim Fonds. The Hyman laboratory acknowledges funding by the European Community's Seventh Framework Program FP7/2007-2013 under grant agreement no. 241548 (MitoSys). M.A. Lampson acknowledges funding by the National Institutes of Health (GM083988).

Author contributions: C. Wurzenberger performed all experiments, analyzed the data, and wrote the paper. M. Held implemented imaging software. M.A. Lampson generated FRET biosensors. A.A. Hyman and I. Poser generated stable cell lines. D.W. Gerlich conceived the project, analyzed data, and wrote the paper.

Submitted: 20 December 2011

Accepted: 13 June 2012

## References

- Akiyoshi, B., K.K. Sarangapani, A.F. Powers, C.R. Nelson, S.L. Reichow, H. Arellano-Santoyo, T. Gonen, J.A. Ranish, C.L. Asbury, and S. Biggins. 2010. Tension directly stabilizes reconstituted kinetochore-microtubule attachments. *Nature*. 468:576–579. <http://dx.doi.org/10.1038/nature09594>
- Bishop, J.D., and J.M. Schumacher. 2002. Phosphorylation of the carboxyl terminus of inner centromere protein (INCENP) by the Aurora B Kinase stimulates Aurora B kinase activity. *J. Biol. Chem.* 277:27577–27580. <http://dx.doi.org/10.1074/jbc.C200307200>
- Civelekoglu-Scholey, G., and J.M. Scholey. 2010. Mitotic force generators and chromosome segregation. *Cell. Mol. Life Sci.* 67:2231–2250. <http://dx.doi.org/10.1007/s00018-010-0326-6>
- DeLuca, K.F., S.M. Lens, and J.G. DeLuca. 2011. Temporal changes in Hec1 phosphorylation control kinetochore-microtubule attachment stability during mitosis. *J. Cell Sci.* 124:622–634. <http://dx.doi.org/10.1242/jcs.072629>
- Dinischiotu, A., M. Beullens, W. Stalmans, and M. Bollen. 1997. Identification of sds22 as an inhibitory subunit of protein phosphatase-1 in rat liver nuclei. *FEBS Lett.* 402:141–144. [http://dx.doi.org/10.1016/S0014-5793\(96\)01514-1](http://dx.doi.org/10.1016/S0014-5793(96)01514-1)
- Fuller, B.G., M.A. Lampson, E.A. Foley, S. Rosasco-Nitcher, K.V. Le, P. Tobelmann, D.L. Brautigam, P.T. Stukenberg, and T.M. Kapoor. 2008. Midzone activation of aurora B in anaphase produces an intracellular phosphorylation gradient. *Nature*. 453:1132–1136. <http://dx.doi.org/10.1038/nature06923>
- Ganem, N.J., Z. Storchova, and D. Pellman. 2007. Tetraploidy, aneuploidy and cancer. *Curr. Opin. Genet. Dev.* 17:157–162. <http://dx.doi.org/10.1016/j.gde.2007.02.011>
- Girdler, F., K.E. Gascoigne, P.A. Eyers, S. Hartmuth, C. Crafter, K.M. Foote, N.J. Keen, and S.S. Taylor. 2006. Validating Aurora B as an anti-cancer drug target. *J. Cell Sci.* 119:3664–3675. <http://dx.doi.org/10.1242/jcs.03145>
- Gruneberg, U., R. Neef, R. Honda, E.A. Nigg, and F.A. Barr. 2004. Relocation of Aurora B from centromeres to the central spindle at the metaphase to anaphase transition requires MKlp2. *J. Cell Biol.* 166:167–172. <http://dx.doi.org/10.1083/jcb.200403084>
- Hauf, S., R.W. Cole, S. LaTerra, C. Zimmer, G. Schnapp, R. Walter, A. Heckel, J. van Meel, C.L. Rieder, and J.M. Peters. 2003. The small molecule Hesperadin reveals a role for Aurora B in correcting kinetochore-microtubule attachment and in maintaining the spindle assembly checkpoint. *J. Cell Biol.* 161:281–294. <http://dx.doi.org/10.1083/jcb.200208092>
- Held, M., M.H. Schmitz, B. Fischer, T. Walter, B. Neumann, M.H. Olma, M. Peter, J. Ellenberg, and D.W. Gerlich. 2010. CellCognition: Time-resolved phenotype annotation in high-throughput live cell imaging. *Nat. Methods*. 7:747–754. <http://dx.doi.org/10.1038/nmeth.1486>
- Honda, R., R. Körner, and E.A. Nigg. 2003. Exploring the functional interactions between Aurora B, INCENP, and survivin in mitosis. *Mol. Biol. Cell.* 14:3325–3341. <http://dx.doi.org/10.1091/mbc.E02-11-0769>
- Hümmer, S., and T.U. Mayer. 2009. Cdk1 negatively regulates midzone localization of the mitotic kinesin Mklp2 and the chromosomal passenger complex. *Curr. Biol.* 19:607–612. <http://dx.doi.org/10.1016/j.cub.2009.02.046>
- Jaqaman, K., E.M. King, A.C. Amaro, J.R. Winter, J.F. Dorn, H.L. Elliott, N. McHedlishvili, S.E. McClelland, I.M. Porter, M. Posch, et al. 2010. Kinetochore alignment within the metaphase plate is regulated by centromere stiffness and microtubule depolymerases. *J. Cell Biol.* 188:665–679. <http://dx.doi.org/10.1083/jcb.200909005>
- Kim, Y., A.J. Holland, W. Lan, and D.W. Cleveland. 2010. Aurora kinases and protein phosphatase 1 mediate chromosome congression through regulation of CENP-E. *Cell*. 142:444–455. <http://dx.doi.org/10.1016/j.cell.2010.06.039>
- Kline, S.L., I.M. Cheeseman, T. Hori, T. Fukagawa, and A. Desai. 2006. The human Mis12 complex is required for kinetochore assembly and proper chromosome segregation. *J. Cell Biol.* 173:9–17. <http://dx.doi.org/10.1083/jcb.200509158>
- Lampson, M.A., and I.M. Cheeseman. 2011. Sensing centromere tension: Aurora B and the regulation of kinetochore function. *Trends Cell Biol.* 21:133–140. <http://dx.doi.org/10.1016/j.tcb.2010.10.007>
- Lampson, M.A., K. Renduchitala, A. Khodjakov, and T.M. Kapoor. 2004. Correcting improper chromosome-spindle attachments during cell division. *Nat. Cell Biol.* 6:232–237. <http://dx.doi.org/10.1038/ncb1102>
- Liu, D., M. Vleugel, C.B. Backer, T. Hori, T. Fukagawa, I.M. Cheeseman, and M.A. Lampson. 2010. Regulated targeting of protein phosphatase 1 to the outer kinetochore by KNL1 opposes Aurora B kinase. *J. Cell Biol.* 188:809–820. <http://dx.doi.org/10.1083/jcb.201001006>
- MacKelvie, S.H., P.D. Andrews, and M.J. Stark. 1995. The *Saccharomyces cerevisiae* gene SDS22 encodes a potential regulator of the mitotic function of yeast type 1 protein phosphatase. *Mol. Cell. Biol.* 15:3777–3785.
- Mirchenko, L., and F. Uhlmann. 2010. Sli15(INCENP) dephosphorylation prevents mitotic checkpoint reengagement due to loss of tension at anaphase onset. *Curr. Biol.* 20:1396–1401. <http://dx.doi.org/10.1016/j.cub.2010.06.023>
- Mochida, S., S. Ikeo, J. Gannon, and T. Hunt. 2009. Regulated activity of PP2A-B55 delta is crucial for controlling entry into and exit from mitosis in *Xenopus* egg extracts. *EMBO J.* 28:2777–2785. <http://dx.doi.org/10.1038/emboj.2009.238>
- Murnion, M.E., R.R. Adams, D.M. Callister, C.D. Allis, W.C. Earnshaw, and J.R. Swedlow. 2001. Chromatin-associated protein phosphatase 1 regulates

- aurora-B and histone H3 phosphorylation. *J. Biol. Chem.* 276:26656–26665. <http://dx.doi.org/10.1074/jbc.M102288200>
- Musacchio, A., and E.D. Salmon. 2007. The spindle-assembly checkpoint in space and time. *Nat. Rev. Mol. Cell Biol.* 8:379–393. <http://dx.doi.org/10.1038/nrm2163>
- Ohkura, H., and M. Yanagida. 1991. *S. pombe* gene *sds22+* essential for a mid-mitotic transition encodes a leucine-rich repeat protein that positively modulates protein phosphatase-1. *Cell.* 64:149–157. [http://dx.doi.org/10.1016/0092-8674\(91\)90216-L](http://dx.doi.org/10.1016/0092-8674(91)90216-L)
- Oliveira, R.A., R.S. Hamilton, A. Pauli, I. Davis, and K. Nasmyth. 2010. Cohesin cleavage and Cdk inhibition trigger formation of daughter nuclei. *Nat. Cell Biol.* 12:185–192. <http://dx.doi.org/10.1038/ncb2018>
- Pereira, G., and E. Schiebel. 2003. Separase regulates INCENP-Aurora B anaphase spindle function through Cdc14. *Science.* 302:2120–2124. <http://dx.doi.org/10.1126/science.1091936>
- Posch, M., G.A. Khoudoli, S. Swift, E.M. King, J.G. Deluca, and J.R. Swedlow. 2010. Sds22 regulates aurora B activity and microtubule–kinetochore interactions at mitosis. *J. Cell Biol.* 191:61–74. <http://dx.doi.org/10.1083/jcb.200912046>
- Poser, I., M. Sarov, J.R. Hutchins, J.K. Hériché, Y. Toyoda, A. Pozniakovskiy, D. Weigl, A. Nitzsche, B. Hegemann, A.W. Bird, et al. 2008. BAC TransgeneOmics: A high-throughput method for exploration of protein function in mammals. *Nat. Methods.* 5:409–415. <http://dx.doi.org/10.1038/nmeth.1199>
- Qian, J., B. Lesage, M. Beullens, A. Van Eynde, and M. Bollen. 2011. PP1/Repo-man dephosphorylates mitotic histone H3 at T3 and regulates chromosomal aurora B targeting. *Curr. Biol.* 21:766–773. <http://dx.doi.org/10.1016/j.cub.2011.03.047>
- Ramadan, K., R. Bruderer, F.M. Spiga, O. Popp, T. Baur, M. Gotta, and H.H. Meyer. 2007. Cdc48/p97 promotes reformation of the nucleus by extracting the kinase Aurora B from chromatin. *Nature.* 450:1258–1262. <http://dx.doi.org/10.1038/nature06388>
- Renouf, S., M. Beullens, S. Wera, A. Van Eynde, J. Sikela, W. Stalmans, and M. Bollen. 1995. Molecular cloning of a human polypeptide related to yeast *sds22*, a regulator of protein phosphatase-1. *FEBS Lett.* 375:75–78. [http://dx.doi.org/10.1016/0014-5793\(95\)01180-M](http://dx.doi.org/10.1016/0014-5793(95)01180-M)
- Ruchaud, S., M. Carmena, and W.C. Earnshaw. 2007. Chromosomal passengers: Conducting cell division. *Nat. Rev. Mol. Cell Biol.* 8:798–812. <http://dx.doi.org/10.1038/nrm2257>
- Salimian, K.J., E.R. Ballister, E.M. Smoak, S. Wood, T. Panchenko, M.A. Lampson, and B.E. Black. 2011. Feedback control in sensing chromosome biorientation by the Aurora B kinase. *Curr. Biol.* 21:1158–1165. <http://dx.doi.org/10.1016/j.cub.2011.06.015>
- Sassoon, I., F.F. Severin, P.D. Andrews, M.R. Taba, K.B. Kaplan, A.J. Ashford, M.J. Stark, P.K. Sorger, and A.A. Hyman. 1999. Regulation of *Saccharomyces cerevisiae* kinetochores by the type 1 phosphatase Glc7p. *Genes Dev.* 13:545–555. <http://dx.doi.org/10.1101/gad.13.5.545>
- Schmitz, M.H., and D.W. Gerlich. 2009. Automated live microscopy to study mitotic gene function in fluorescent reporter cell lines. *Methods Mol. Biol.* 545:113–134. [http://dx.doi.org/10.1007/978-1-60327-993-2\\_7](http://dx.doi.org/10.1007/978-1-60327-993-2_7)
- Schmitz, M.H., M. Held, V. Janssens, J.R. Hutchins, O. Hudecz, E. Ivanova, J. Goris, L. Trinkle-Mulcahy, A.I. Lamond, I. Poser, et al. 2010. Live-cell imaging RNAi screen identifies PP2A-B55alpha and importin-beta1 as key mitotic exit regulators in human cells. *Nat. Cell Biol.* 12:886–893. <http://dx.doi.org/10.1038/ncb2092>
- Sessa, F., M. Mapelli, C. Ciferri, C. Tarricone, L.B. Areces, T.R. Schneider, P.T. Stukenberg, and A. Musacchio. 2005. Mechanism of Aurora B activation by INCENP and inhibition by hesperadin. *Mol. Cell.* 18:379–391. <http://dx.doi.org/10.1016/j.molcel.2005.03.031>
- Steigemann, P., C. Wurzenberger, M.H. Schmitz, M. Held, J. Guizetti, S. Maar, and D.W. Gerlich. 2009. Aurora B-mediated abscission checkpoint protects against tetraploidization. *Cell.* 136:473–484. <http://dx.doi.org/10.1016/j.cell.2008.12.020>
- Stone, E.M., H. Yamano, N. Kinoshita, and M. Yanagida. 1993. Mitotic regulation of protein phosphatases by the fission yeast *sds22* protein. *Curr. Biol.* 3:13–26. [http://dx.doi.org/10.1016/0960-9822\(93\)90140-J](http://dx.doi.org/10.1016/0960-9822(93)90140-J)
- Sugiyama, K., K. Sugiura, T. Hara, K. Sugimoto, H. Shima, K. Honda, K. Furukawa, S. Yamashita, and T. Urano. 2002. Aurora-B associated protein phosphatases as negative regulators of kinase activation. *Oncogene.* 21:3103–3111. <http://dx.doi.org/10.1038/sj.onc.1205432>
- Sumara, I., M. Quadroni, C. Frei, M.H. Olma, G. Sumara, R. Ricci, and M. Peter. 2007. A Cul3-based E3 ligase removes Aurora B from mitotic chromosomes, regulating mitotic progression and completion of cytokinesis in human cells. *Dev. Cell.* 12:887–900. <http://dx.doi.org/10.1016/j.devcel.2007.03.019>
- Tanaka, T.U., N. Rachidi, C. Janke, G. Pereira, M. Galova, E. Schiebel, M.J. Stark, and K. Nasmyth. 2002. Evidence that the Ipl1-Sli15 (Aurora kinase-INCENP) complex promotes chromosome bi-orientation by altering kinetochore-spindle pole connections. *Cell.* 108:317–329. [http://dx.doi.org/10.1016/S0092-8674\(02\)00633-5](http://dx.doi.org/10.1016/S0092-8674(02)00633-5)
- Trinkle-Mulcahy, L., J. Andersen, Y.W. Lam, G. Moorhead, M. Mann, and A.I. Lamond. 2006. Repo-Man recruits PP1γ to chromatin and is essential for cell viability. *J. Cell Biol.* 172:679–692. <http://dx.doi.org/10.1083/jcb.200508154>
- Vagnarelli, P., D.F. Hudson, S.A. Ribeiro, L. Trinkle-Mulcahy, J.M. Spence, F. Lai, C.J. Farr, A.I. Lamond, and W.C. Earnshaw. 2006. Condensin and Repo-Man-PP1 co-operate in the regulation of chromosome architecture during mitosis. *Nat. Cell Biol.* 8:1133–1142. <http://dx.doi.org/10.1038/ncb1475>
- Vagnarelli, P., S. Ribeiro, L. Sennels, L. Sanchez-Pulido, F. de Lima Alves, T. Verheyen, D.A. Kelly, C.P. Ponting, J. Rappsilber, and W.C. Earnshaw. 2011. Repo-Man coordinates chromosomal reorganization with nuclear envelope reassembly during mitotic exit. *Dev. Cell.* 21:328–342. <http://dx.doi.org/10.1016/j.devcel.2011.06.020>
- Vázquez-Novelle, M.D., and M. Petronczki. 2010. Relocation of the chromosomal passenger complex prevents mitotic checkpoint engagement at anaphase. *Curr. Biol.* 20:1402–1407. <http://dx.doi.org/10.1016/j.cub.2010.06.036>
- Walczak, C.E., S. Cai, and A. Khodjakov. 2010. Mechanisms of chromosome behaviour during mitosis. *Nat. Rev. Mol. Cell Biol.* 11:91–102. <http://dx.doi.org/10.1038/nrg2737>
- Wang, W., P.T. Stukenberg, and D.L. Brautigan. 2008. Phosphatase inhibitor-2 balances protein phosphatase 1 and aurora B kinase for chromosome segregation and cytokinesis in human retinal epithelial cells. *Mol. Biol. Cell.* 19:4852–4862. <http://dx.doi.org/10.1091/mbc.E08-05-0460>
- Welburn, J.P., M. Vleugel, D. Liu, J.R. Yates III, M.A. Lampson, T. Fukagawa, and I.M. Cheeseman. 2010. Aurora B phosphorylates spatially distinct targets to differentially regulate the kinetochore-microtubule interface. *Mol. Cell.* 38:383–392. <http://dx.doi.org/10.1016/j.molcel.2010.02.034>
- Yasui, Y., T. Urano, A. Kawajiri, K. Nagata, M. Tatsuka, H. Saya, K. Furukawa, T. Takahashi, I. Izawa, and M. Inagaki. 2004. Autophosphorylation of a newly identified site of Aurora-B is indispensable for cytokinesis. *J. Biol. Chem.* 279:12997–13003. <http://dx.doi.org/10.1074/jbc.M311128200>